fluids

MDPI

Article

Analysis and Modelling of the Commutation Error

Markus Klein [1,*] **and Massimo Germano** [2]

[1] Department of Aerospace Engineering, Bundeswehr University Munich, Werner-Heisenberg-Weg 39, 85577 Neubiberg, Germany
[2] Department of Civil and Environmental Engineering, Duke University, Durham, NC 27708, USA; mg234@duke.edu
* Correspondence: markus.klein@unibw.de; Tel.:+49-89-6004-2122

Abstract: A multiscale dynamic analysis of the commutation error, based on the filtering approach is performed. The similarity multiscale hypothesis proposed by Bardina (1983) and extended by Geurts and Holm (2006) to the commutation error is examined in detail and an extension of the Germano identity to the analysis and the modelling of the commutation error is proposed. For a detailed analysis under controlled condition the method is first applied to synthetic turbulence and subsequently to the a-priori analysis of a turbulent channel flow at $Re_\tau = 590$. The results illustrate the flexibility of the dynamic modelling approach. Combined with a scale similarity assumption for the commutation error very satisfactory results have been obtained for first order derivatives and reasonable results for second order derivatives. In all cases the modelling of the commutation error resulted in smaller errors than the error obtained by neglecting the commutation error.

Keywords: large eddy simulation; commutation error; dynamic modelling; scale similarity model; a-priori analysis

Citation: Klein, M.; Germano, M. Analysis and Modelling of the Commutation Error. *Fluids* **2021**, *6*, 15. https://doi.org/10.3390/fluids6010015

Received: 08 December 2020
Accepted: 24 December 2020
Published: 31 December 2020

1. Introduction

Turbulence modelling using the Large Eddy Simulation (LES) technique is considered advantageous over traditional methods relying on Reynolds averaging due to its inherent ability to resolve the energy carrying turbulent structures. Given the advances in computing power over the last decades, together with recent advances in numerical methods [1,2] and advanced modelling techniques [3,4] based on machine learning, it can be expected that LES will be increasingly used in the future for a variety of applications such as combustion [5,6] or two-phase flows [7–9] to name only two.

The Large Eddy Simulation of turbulent flow is affected by many errors, due to many reasons, first of all the granularity of the grid coupled with the nonlinearity of the equations. Following Reference [10], we can formalize all that in terms of a filtering approach that reads the data produced by a numerical code as a filtered database. The filtering operator representative of a given LES is characterized by a filter length, directly associated to the grid length, and a lot of information, useful both for modelling and for analysing the results, can be recovered by comparing two different simulations at two different resolution levels by means of the so called dynamic filtering approach. As recalled in the abstract, the first application of the dynamic modelling approach was presented thirty years ago at the Summer Meeting of the CTR [11], and since then a lot of different applications flourished thanks to the interest of many researchers around the world. We refer both to the cited Reference [12] and to Reference [13] for more details on that.

In order to derive the LES formalism, the Navier-Stokes equations are usually filtered with a commutative filter, that is, $\partial\overline{u} = \overline{\partial u}$ where u denotes a general variable and $\bar{\cdot}$ a

general filtering operation, typically defined as a convolution integral (here for illustration in 1D) with the filter kernel G such that

$$\overline{u}(x) = \int_{-\infty}^{\infty} u(y)G(x-y)dy, \quad \int_{-\infty}^{\infty} G(x-y)dy = 1. \tag{1}$$

Examples of filter kernels in physical scace are the box filter

$$G(x-y) = \frac{1}{\Delta} \text{ if } |x-y| \leq \frac{\Delta}{2}; \quad G(x-y) = 0 \text{ otherwise} \tag{2}$$

or the Gaussian filter

$$G(x-y) = \left(\frac{6}{\pi\Delta^2}\right)^{1/2} exp\left(\frac{-6|x-y|^2}{\Delta^2}\right). \tag{3}$$

Making use of the linearity of filtering one obtains

$$\frac{\partial}{\partial t}\overline{u_i} = -\frac{\partial}{\partial x_j}\left(\overline{u_i u_j}\right) + \frac{\partial}{\partial x_j}\nu\left(\frac{\partial \overline{u_i}}{\partial x_j} + \frac{\partial \overline{u_j}}{\partial x_i}\right) - \frac{1}{\rho}\frac{\partial \overline{p}}{\partial x_i}. \tag{4}$$

Without loss of generality viscosity ν and density ρ are assumed to be constant. Two approaches exist to deal with the unknown correlation $\overline{u_i u_j}$ appearing in the filtered Navier-Stokes equations [14]:

$$\overline{u_i u_j} = \overline{u_i}\,\overline{u_j} + \left(\overline{u_i u_j} - \overline{u_i}\,\overline{u_j}\right) \tag{5}$$

$$\overline{u_i u_j} = \overline{\overline{u_i}\,\overline{u_j}} + \left(\overline{u_i u_j} - \overline{\overline{u_i}\,\overline{u_j}}\right). \tag{6}$$

The term in parentheses is the unknown sgs stress tensor τ_{ij}. If Equation (5) is used, a closed equation for $\overline{u_i}$ is obtained, provided a model for τ_{ij} is supplied. This equation requires no explicit filtering during the solution process. If relation (6) is used one obtains again a closed equation but this time with an additional explicit filtering operation applied to the non linear term. Therefore we call the first approach implicit filtering and the second approach explicit filtering ([15] uses the terminology triple and double decomposition).

In order to derive Equation (4) a homogeneous filter defined in an infinite domain has been assumed. Problems with the theory outlined so far can therefore arise from inhomogeneous filters or from bounded computational domains. This can be seen by differentiating Equation (1) with respect to x which gives [15]:

$$\frac{\partial \overline{u}(x)}{\partial x} = \overline{\frac{\partial u(x)}{\partial x}} + \int_{-\infty}^{\infty} u(y)\frac{\partial G(x-y)}{\partial x}dy. \tag{7}$$

Inhomogeneous filters (grids) are extensively applied in the proximity of walls or regions of strong gradients, like shear layers for example. Hence, the commutation of derivation and filtering is of particular importance for manipulating the Navier-Stokes equations and application of a non commutative filter to the governing equations results in unknown expressions for all terms.

The problem of deriving high order commutative (HOC) filters has been addressed in the past literature (e.g., References [16–18]). Vasilyev et al. [17] developed a class of HOC filters using a mapping function. In extension to that work Marsden et al. [18] proposed a more general procedure for use on unstructured meshes. These filters are defined as a linear combination of simple commutative basis filters, thus allowing to control additionally the filter shape. An implementation of this method into an unstructured solver can for example be found in Reference [19]. The underlying idea of the work mentioned above is that the commutation error can be controlled by imposing conditions on the filter moments.

However, as the primary filtering operation is not explicitly performed in a real LES [14], a general limitation of these ideas is, that these commutative filters can only be used for the secondary filtering operation, such as in Equation (6), or when using a test filter in the dynamic modelling approach. John [20] argues that the commutation error vanishes if and only if the normal stress on the boundary is zero for all times which is very unlikely. While the analysis in this work considers only spatial, time independent filters, it is worth to mention the following extensions: Leonard et al. [21] discuss the commutation error when the spatial filter varies in time, while Franke and Frank analyse the temporal commutation error [22]. The next sections discuss a framework that potentially could be used for modelling the commutation error for the primary filtering operation such as in Equation (5).

2. Multiscale Modelling

It has been mentioned in Reference [23] that the commutation error can be modelled using a scale similarity type approach. Here the main attention is not only to modelling but equally important to analyse the commutation errors with the filtering approach and the related multiscale procedure based on the Germano identity. We remark that in the framework of the filtering approach a Large Eddy Simulation of a turbulent flow is mathematically formalized as a filtered representation of a Direct Simulation. If with $\mathcal{F}$ we represent the filtering operator usually unknown and denoted with an overbar $\bar{\cdot}$, that produces the filtered LES values $\langle u_i \rangle_f$ of the velocity components, a basic problem is to understand how the filtered product $\langle u_i u_j \rangle_f$ is related to them. The filtering approach tries to resolve this problem from a multiscale point of view. We define the Generalized Central Moment, (GCM), $\tau_f(u_i, u_j)$ associated to $\langle u_i u_j \rangle_f$ as

$$\tau_f(u_i, u_j) = \langle u_i u_j \rangle_f - \langle u_i \rangle_f \langle u_j \rangle_f, \tag{8}$$

and we look to the GCM associated to $\langle \langle u_i u_j \rangle_f \rangle_g$, where $\mathcal{G}$ is an explicit test filtering operator, denoted also with a hat $\hat{\cdot}$,

$$\tau_{fg}(u_i, u_j) = \langle \langle u_i u_j \rangle_f \rangle_g - \langle \langle u_i \rangle_f \rangle_g \langle \langle u_j \rangle_f \rangle_g. \tag{9}$$

It is easy to see that the *resolved* GCM (based on resolved quantities $\langle \cdot \rangle_f$ and considering filter level g),

$$\tau_g(\langle u_i \rangle_f, \langle u_j \rangle_f) = \langle \langle u_i \rangle_f \langle u_j \rangle_f \rangle_g - \langle \langle u_i \rangle_f \rangle_g \langle \langle u_j \rangle_f \rangle_g \tag{10}$$

can alternatively be expressed by the tensor M_{ij} defined as

$$M_{ij} = \tau_{fg}(u_i, u_j) - \langle \tau_f(u_i, u_j) \rangle_g. \tag{11}$$

Inserting a model expression for τ_f and τ_{fg} with one free model parameter into Equation (11) to express M_{ij} and equating it to Equation (10) one could in principle determine this model parameter from

$$\tau_g(\langle u_i \rangle_f, \langle u_j \rangle_f) = M_{ij}. \tag{12}$$

However, each tensor component would provide a different equation and a different value of for the model parameter. If instead we contract the identity (12) with M_{ij}, following the approach of Lilly [24], we have identically

$$\tau_g(\langle u_i \rangle_f, \langle u_j \rangle_f) M_{ij} = M_{ij} M_{ij}\,. \tag{13}$$

The contraction corresponds to summation over both indices and as a result of it the resulting model parameter represents the single model parameter which provides the best

approximation in a least square sense to the six equations representing the symmetric tensor components.

We remark that from the LES modelling point of view, but not only, it is very important to understand how the dynamic coefficient C

$$C = \frac{\tau_g(\langle u_i\rangle_f, \langle u_j\rangle_f)M_{ij}}{M_{ij}M_{ij}} \tag{14}$$

scales with resolved quantities. Obviously the dynamic coefficient C should be rigorously equal to one everywhere if the modelling scaling is exact, but this is not the case for a generic scaling model. As an example, we can scale M_{ij} with the similarity model of Bardina [25].

Thus we can write

$$\begin{aligned}
\tau_{ss,f}(u_i,u_j) &= \tau_f(\langle u_i\rangle_f, \langle u_j\rangle_f) = \\
&= \langle\langle u_i\rangle_f\langle u_j\rangle_f\rangle_f - \langle\langle u_i\rangle_f\rangle_f\langle\langle u_j\rangle_f\rangle_f \\
&= \overline{\overline{u_i}\,\overline{u_i}} - \overline{\overline{u_i}}\,\overline{\overline{u_j}} \qquad (15)\\
\tau_{ss,fg}(u_i,u_j) &= \tau_{fg}(\langle u_i\rangle_{fg}, \langle u_j\rangle_{fg}) \\
&= \langle\langle u_i\rangle_{fg}\langle u_j\rangle_{fg}\rangle_{fg} - \langle\langle u_i\rangle_{fg}\rangle_{fg}\langle\langle u_j\rangle_{fg}\rangle_{fg} \\
&= \widehat{\overline{\widehat{u_i}}\,\overline{\widehat{u_i}}} - \overline{\widehat{u_i}}\,\overline{\widehat{u_j}} \qquad (16)
\end{aligned}$$

and finally the parameter C_{ss} be computed with *resolved* quantities

$$C_{ss} = \frac{\tau_g(\langle u_i\rangle_f, \langle u_j\rangle_f)M_{ss,ij}}{M_{ss,ij}M_{ss,ij}} \tag{17}$$

where

$$M_{ss,ij} = \tau_{ss,fg}(u_i,u_j) - \langle\tau_{ss,f}(u_i,u_j)\rangle_g. \tag{18}$$

In this local form, the Bardina dynamic coefficient C_{ss} depends on time and space, but a global form can be conceived, averaged in time and/or eventually in homogeneous space directions.

Strangely enough this multiscale approach and the main use of the identity (12) was to *model* turbulence, and not to *analyse* its multiscale peculiarities. The reasons for that are not so simple to explain. We only remark that this attitude has prevented simple observations that could be usefully applied to LES. One of them refers to the commutation error, and that is the main contribution of this paper. Let us formally consider the GCM associated to the filtered product of a space derivative with a velocity component $\langle\partial_j u_i\rangle_f$, on filter level $\mathcal{F}$ defined as

$$\tau_f(\partial_i,u_j) = \langle\partial_i u_j\rangle_f - \partial_i\langle u_j\rangle_f = \overline{\frac{\partial u}{\partial x}} - \frac{\partial\overline{u}}{\partial x}. \tag{19}$$

If we introduce once more an explicit test filter $\mathcal{G}$, a simple extension of the identity (12) is the following

$$\tau_g(\partial_i,\langle u_j\rangle_f) = \tau_{fg}(\partial_i,u_j) - \langle\tau_f(\partial_i,u_j)\rangle_g = \left(\frac{\widehat{\partial\overline{u}}}{\partial x} - \frac{\partial\widehat{\overline{u}}}{\partial x}\right) - \left(\widehat{\overline{\frac{\partial u}{\partial x}}} - \frac{\partial\overline{u}}{\partial x}\right), \tag{20}$$

where $\tau_g(\partial_i,\langle u_j\rangle_f)$ is the *resolved* GCM given by

$$\tau_g(\partial_i,\langle u_j\rangle_f) = \langle\partial_i\langle u_j\rangle_f\rangle_g - \partial_i\langle u_j\rangle_{fg} = \left(\frac{\widehat{\partial\overline{u}}}{\partial x} - \frac{\partial\widehat{\overline{u}}}{\partial x}\right). \tag{21}$$

We can contract this identity like

$$\tau_g(\partial_i, \langle u_j \rangle_f) M_{ij} = M_{ij} M_{ij}, \tag{22}$$

where

$$M_{ij} = \tau_{fg}(\partial_i, u_j) - \langle \tau_f(\partial_i, u_j) \rangle_g = \left(\widehat{\frac{\partial \overline{u}}{\partial x}} - \frac{\partial \widehat{\overline{u}}}{\partial x} \right) - \left(\widehat{\frac{\partial u}{\partial x}} - \frac{\partial \overline{u}}{\partial x} \right) \tag{23}$$

and also in this case it is very important to understand how the dynamic coefficient C associated to the commutation GCM,

$$C = \frac{\tau_g(\partial_i, \langle u_j \rangle_f) M_{ij}}{M_{ij} M_{ij}} \tag{24}$$

scales with resolved quantities. Obviously the candidates to this explorations are many. The scale similarity model is known to show high correlations in a-priori tests not only for isothermal flows but also for the stress, the flux modelling and the reaction rate closure in reacting flows [26–28] or two phase flows [7,8]. The problem of insufficient dissipation of the model has for example been addressed in Reference [29]. Encouraged by these results and by the work of Reference [23] we will therefore examine in some detail how the ratio C scales with the extension of the similarity model of Bardina [25]. We write

$$\tau_{ss,f}(\partial_i, \langle u_j \rangle_f) = \langle \partial_i \langle u_j \rangle_f \rangle_f - \partial_i \langle \langle u_j \rangle_f \rangle_f = C \left(\frac{\partial \overline{\overline{u}}}{\partial x} - \frac{\partial \overline{\overline{u}}}{\partial x} \right) \tag{25}$$

$$\tau_{ss,fg}(\partial_i, \langle u_j \rangle_{fg}) = \langle \partial_i \langle u_j \rangle_{fg} \rangle_{fg} - \partial_i \langle \langle u_j \rangle_{fg} \rangle_{fg} = C \left(\frac{\partial \widehat{\overline{\overline{u}}}}{\partial x} - \frac{\partial \widehat{\overline{\overline{u}}}}{\partial x} \right) \tag{26}$$

as well as

$$M_{ss,ij} = \tau_{ss,fg}(\partial_i, u_j) - \langle \tau_{ss,f}(\partial_i, u_j) \rangle_g \tag{27}$$

such that finally

$$\begin{aligned} C_{ss} &= \frac{\tau_g(\partial_i, \langle u_j \rangle_f) M_{ss,ij}}{M_{ss,ij} M_{ss,ij}} \\ &= \frac{\left(\widehat{\frac{\partial \overline{\overline{u}}}{\partial x}} - \frac{\partial \widehat{\overline{\overline{u}}}}{\partial x} \right) \times \left[\left(\widehat{\frac{\partial \overline{\overline{u}}}{\partial x}} - \frac{\partial \widehat{\overline{\overline{u}}}}{\partial x} \right) - \left(\widehat{\frac{\partial \overline{\overline{u}}}{\partial x}} - \frac{\partial \overline{\overline{u}}}{\partial x} \right) \right]}{\left[\left(\widehat{\frac{\partial \overline{\overline{u}}}{\partial x}} - \frac{\partial \widehat{\overline{\overline{u}}}}{\partial x} \right) - \left(\widehat{\frac{\partial \overline{\overline{u}}}{\partial x}} - \frac{\partial \overline{\overline{u}}}{\partial x} \right) \right] \times \left[\left(\widehat{\frac{\partial \overline{\overline{u}}}{\partial x}} - \frac{\partial \widehat{\overline{\overline{u}}}}{\partial x} \right) - \left(\widehat{\frac{\partial \overline{\overline{u}}}{\partial x}} - \frac{\partial \overline{\overline{u}}}{\partial x} \right), \right]} \end{aligned} \tag{28}$$

where numerator and denominator will be space or ensemble averaged as appropriate. Averaging is a standard procedure for regularisation of the dynamic procedure (for an overview on this topic see Reference [15]). For unsteady 3D flow problems the averaging in homogeneous directions can be replaced by the Lagrangian dynamic model proposed by Meneveau et al. [30].

3. Approximations for Commutation Errors

In this section a first order approximation of the commutation error for the first and second derivative will be presented under the assumption that the filter is a differential or elliptic filter. If the filter varies in space and the filter width is formally associated to the length scale Δ one can explicitly include this dependency in Equation (7)

$$\begin{aligned}\frac{\partial \overline{u}(x,t,\Delta)}{\partial x} &= \overline{\frac{\partial u(x,t,\Delta)}{\partial x}} + \int_{-\infty}^{\infty} \frac{\partial G(\xi,\Delta)}{\partial x} u(x-\xi,t)d\xi \\ &= \overline{\frac{\partial u(x,t,\Delta)}{\partial x}} + \int_{-\infty}^{\infty} \frac{\partial \Delta}{\partial x}\frac{\partial G(\xi,\Delta)}{\partial \Delta} u(x-\xi,t)d\xi \end{aligned} \tag{29}$$

such that the commutation error can be formally expressed in one dimension as [31,32]

$$\tau_f(\partial,u) \equiv \langle \partial u\rangle_f - \partial\langle u\rangle_f = -\frac{\partial\Delta}{\partial x}\frac{\partial\langle u\rangle_f}{\partial\Delta}. \tag{30}$$

By using the overline notation we derive the following expression for the second order derivative

$$\tau(\partial,u) = \overline{\frac{\partial u}{\partial x}} - \frac{\partial \overline{u}}{\partial x} = -\frac{\partial\Delta}{\partial x}\frac{\partial\overline{u}}{\partial\Delta} \tag{31}$$

$$\tau(\partial,\partial u) = \overline{\frac{\partial}{\partial x}\frac{\partial u}{\partial x}} - \frac{\partial}{\partial x}\overline{\frac{\partial u}{\partial x}} = -\frac{\partial\Delta}{\partial x}\frac{\partial}{\partial\Delta}\overline{\frac{\partial u}{\partial x}} \tag{32}$$

$$\begin{aligned}\tau(\partial^2,u) &= \overline{\frac{\partial^2 u}{\partial x^2}} - \frac{\partial^2\overline{u}}{\partial x^2} \\ &= \frac{\partial\tau(\partial,u)}{\partial x} - \frac{\partial\Delta}{\partial x}\frac{\partial^2\bar{u}}{\partial\Delta\partial x} - \frac{\partial\Delta}{\partial x}\frac{\partial\tau(\partial,u)}{\partial\Delta}. \end{aligned} \tag{33}$$

The commutation error has been also examined in Reference [33]. From this last paper we can derive an estimate of the derivative of $\overline{u}$ with Δ in the case of the *elliptic* differential filter [34]

$$u = \overline{u} - \Delta^2\frac{\partial^2\overline{u}}{\partial x^2}; \qquad \frac{\partial\overline{u}}{\partial\Delta} \sim 2\Delta\frac{\partial^2\bar{u}}{\partial x^2}. \tag{34}$$

In this case we have as a first approximation

$$\tau(\partial,u) \approx \tau_a = -2\Delta\frac{\partial\Delta}{\partial x}\frac{\partial^2\overline{u}}{\partial x^2}. \tag{35}$$

Similarly, the Gaussian filter and its inverse can be approximated by a differential filter [15]

$$u \approx \overline{u} - \frac{1}{24}\Delta^2\frac{\partial^2\overline{u}}{\partial x^2}; \quad \overline{u} \approx u + \frac{1}{24}\Delta^2\frac{\partial^2 u}{\partial x^2} = u + (\Delta^*)^2\frac{\partial^2 u}{\partial x^2}; \quad \Delta^* = (1/24)^{1/2}\Delta. \tag{36}$$

From Equation (31) we get

$$\frac{\partial\tau(\partial,u)}{\partial x} = -\frac{\partial^2\Delta}{\partial x^2}\frac{\partial\bar{u}}{\partial\Delta} - \frac{\partial\Delta}{\partial x}\frac{\partial^2\bar{u}}{\partial\Delta\partial x} \tag{37}$$

$$\frac{\partial\tau(\partial,u)}{\partial\Delta} = -\frac{\partial\Delta}{\partial x}\frac{\partial^2\bar{u}}{\partial\Delta^2} \tag{38}$$

and insertion in Equation (33) gives

$$\overline{\frac{\partial^2 u}{\partial x^2}} - \frac{\partial^2\overline{u}}{\partial x^2} = -2\frac{\partial\Delta}{\partial x}\frac{\partial^2\bar{u}}{\partial\Delta\partial x} - \frac{\partial^2\Delta}{\partial x^2}\frac{\partial\bar{u}}{\partial\Delta} - \left(\frac{\partial\Delta}{\partial x}\right)^2\frac{\partial^2\bar{u}}{\partial\Delta^2}. \tag{39}$$

If, using Equation (34), we write as a first approximation

$$\frac{\partial^2\bar{u}}{\partial x\partial\Delta} = 2\Delta\frac{\partial^3\bar{u}}{\partial x^3} + 2\frac{\partial\Delta}{\partial x}\frac{\partial^2\bar{u}}{\partial x^2} \tag{40}$$

the first term to the right in (39) reads as

$$-2\frac{\partial\Delta}{\partial x}\frac{\partial^2\bar{u}}{\partial\Delta\partial x} = -4\Delta\frac{\partial\Delta}{\partial x}\frac{\partial^3\bar{u}}{\partial x^3} - 4\left(\frac{\partial\Delta}{\partial x}\right)^2\frac{\partial^2\bar{u}}{\partial x^2}. \tag{41}$$

One can assume that $(\partial\Delta/\partial x)^2 < (\partial\Delta/\partial x)$ and $(\partial\Delta/\partial x)^2 < \Delta(\partial\Delta/\partial x)$. Often a constant grid stretching is used such that $\partial\Delta/\partial x = const$ and $\partial^2\Delta/\partial x^2 = 0$. Under these conditions one has

$$\tau(\partial^2, u) =\approx \tau_a^2 = -4\Delta\frac{\partial\Delta}{\partial x}\frac{\partial^3\bar{u}}{\partial x^3}. \tag{42}$$

4. Analysis of Synthetic Turbulence

The commutation for the primary filter affects, apart from the temporal derivative, every term in the Navier-Stokes equations. Hence an implementation of the methodology in a real LES will be cumbersome and not straightforward on bounded domains with non-uniform meshes. For a first illustration of the methodology a simple 1D example has been chosen here, which has also the advantage that all turbulence parameters can be strictly controlled.

4.1. First Order Derivatives

The computational mesh used for illustration of the method is a stretched one-dimensional mesh with variables stored in the cell center on a domain with unity length. The first cell has a length of $\Delta x = \Delta x_1$ and the subsequent cells (50 in total) have the width $\Delta x_i = \Delta x \cdot s^{i-1}$ where s is a constant stretch factor taken as 1.05 for the example in Figure 1. In this particular case the first mesh cell has a width of $\Delta x = \Delta x_1 = 0.00239$. The discrete filter is an inhomogeneous, asymmetric box filter as illustrated in Figure 1.

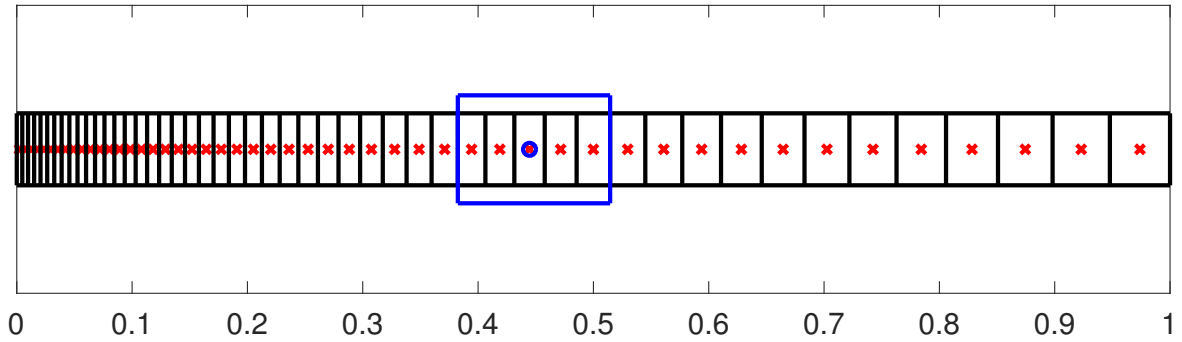

Figure 1. Illustration of the stretched 1D computational mesh with cell centred data storage and one sketched box filter.

For a given parameter p the filter around a point i_0 is given by the coefficients with the weights w_{i_0+i}:

$$w_{i_0+i} = \Delta x_{i_0+i}/w_{tot}, \quad i = -p, \ldots, p, \quad w_{tot} = \sum_{i=-p,\ldots,p} \Delta x_{i_0+i}. \tag{43}$$

All derivatives are calculated by second order accurate finite differences for non-equidistant meshes

$$\frac{\partial u_i}{\partial x} \approx \frac{u_{i+1}\Delta_-^2 - u_{i-1}\Delta_+^2 + u_i(\Delta_+^2 - \Delta_-^2)}{\Delta_-\Delta_+(\Delta_- + \Delta_+)}, \quad \Delta_- = x_i - x_{i-1}, \; \Delta_+ = x_{i+1} - x_i, \tag{44}$$

where x_i denotes the midpoints of the cells. It is worth noting that this formula reduces to the standard central difference for equidistant meshes. Due to the inhomogeneous filtering operation the mesh has to be elongated in positive $(x > 1)$ and negative $(x < 0)$ direction in order to have a well-defined filtering operation for up to fourfold filtering. Pseudo turbulent data has been generated using the digital filter based method detailed in Reference [35], where the integral turbulent length scale has been set to $L_{11} = 5\Delta x_1$

respectively $10\Delta x_1$ and the fluctuation intensity is set to unity without loss of generality. The associated two-point autocorrelation function (an equivalent of the energy spectrum) obtained by this approach resembles homogenous isotropic turbulence in a late stage [35].

The turbulent initial data has been generated on a uniform mesh and interpolated on the non-equidistant computational mesh using a cubic spline function, as illustrated in Figure 2. The derivatives of the signal shown in Figure 2 and the associated commutation error are shown in Figure 3a,b. It is worth noting that for a homogeneous symmetric filter $\tau_f = 0$ and this has been verified in the numerical implementation by setting the stretch factor to $s = 1$. We remark that the numerical gradients become smaller with larger grid size (i.e., towards the right boundary of the computational domain). The scale similarity model given by Equation (25) is shown together with the commutation error in Figure 3b using $C = 1$. Table 1 shows the performance of the model in terms of the Pearson correlation coefficient for initial data with two different length scales and two different filter width, which according to Equation (43) can be specified using the parameter p_f. Furthermore, Table 1 shows the optimal model parameter C determined from a least square fit of the model data to the real commutation error according to Equation (25). The numerical experiment has been repeated 2000 times and all data is space and ensemble averaged. In a real LES determination of the model constant C using least square fits is not possible because the commutation error is unknown. Table 1 shows also the dynamically determined model coefficient C_{ss} for different initial data and different f, g filter size pairs (p_f, p_g). It can be seen that the dynamic procedure reasonably represents the optimal model coefficient. It is also worth mentioning that in all cases the model error, using either the default value $C = 1$ or the optimal value from least square fits, has been found to be considerably smaller than the commutation error (representative of using no model) and this is demonstrated in Table 1 by the relative mean squared error (RMSE) defined as the local mean squared commutation error divided by the local mean squared value of the derivative of the signal multiplied with 100. We remark the simple extension of the dynamic procedure that can be easily generalized and implemented in different directions.

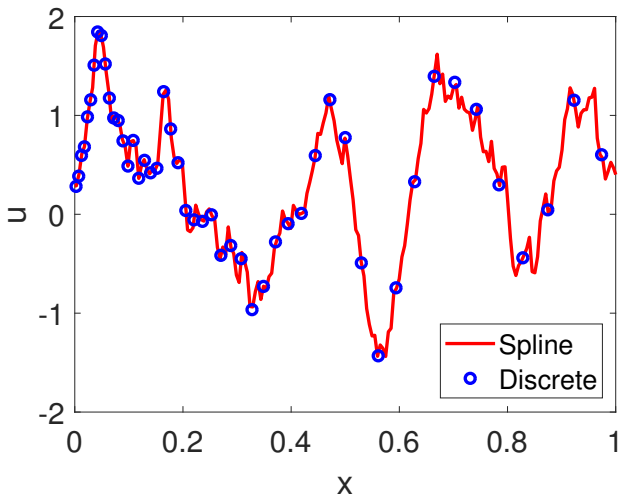

Figure 2. Spline through digital filter based pseudo turbulence and corresponding values interpolated on the computational mesh.

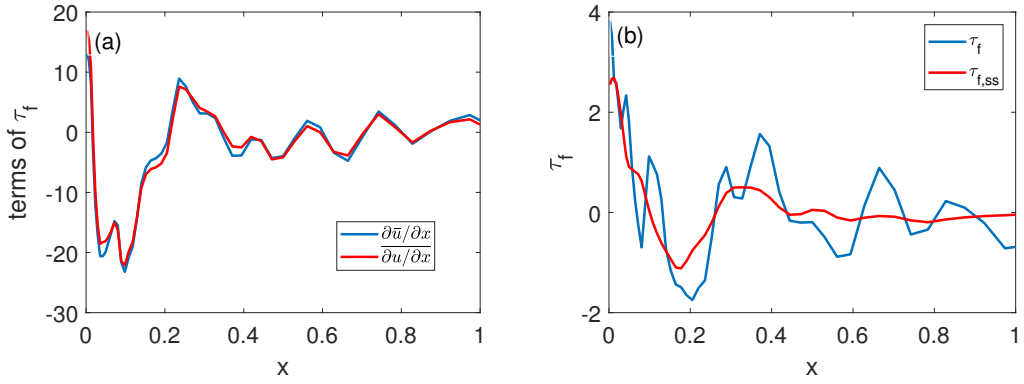

Figure 3. (**a**) (Filtered) gradients of the data (filtered data) shown in Figure 2. (**b**) Commutation error given by $\overline{\partial u/\partial x} - \partial\overline{u}/\partial x$ together with scale similarity model for the commutation error, given by Equation (25) using $C = 1$.

Table 1. Performance of model $\tau_{f,ss}$ for different initial data and different filter sizes (note that the correlation coefficient is independent of the secondary filter). Dynamically determined model coefficient C and mean squared error between commutation error and different approximations, for different initial data and different f, g filter size pairs (p_f, p_g).

Turb. Length Scale L_{11} **Filter Width Pair (p_f, p_g)**	**5Δx** **(1,2)**	**5Δx** **(5,10)**	**10Δx** **(1,2)**	**10Δx** **(5,10)**
Corr. Coeff.	0.90	0.63	0.90	0.71
Opt. C	1.39	1.56	1.37	1.38
C_{ss} dynamic	1.66	1.83	1.51	1.53
RMSE $(\tau_f - 0)$	0.16	6.36	0.09	5.02
RMSE $(\tau_f - \tau_{f,ss}, C = 1)$	0.06	4.80	0.02	3.35
RMSE $(\tau_f - \tau_{f,ss}, C_{opt})$	0.05	4.51	0.01	3.09

4.2. Second Order Derivatives

The same procedure can be automatically extended to the second derivatives. The commutation error is then given by:

$$\tau_f^2 = \overline{\frac{\partial^2 u}{\partial x^2}} - \frac{\partial^2 \overline{u}}{\partial x^2}. \tag{45}$$

The second numerical derivatives are calculated using the following formula:

$$\frac{\partial^2 u_i}{\partial x^2} \approx \frac{2(u_{i+1}\Delta_- + u_{i-1}\Delta_+ - u_i(\Delta_+ + \Delta_-))}{\Delta_-\Delta_+(\Delta_- + \Delta_+)}, \quad \Delta_- = x_i - x_{i-1}, \; \Delta_+ = x_{i+1} - x_i \tag{46}$$

The scale similarity model for the second derivative reads:

$$\tau_{f,ss}^2 = C\left(\overline{\frac{\partial^2 \overline{u}}{\partial x^2}} - \frac{\partial^2 \overline{\overline{u}}}{\partial x^2}\right). \tag{47}$$

The associated filtered second derivatives and second derivatives of filtered data are illustrated in Figure 4a. The scale similarity model given by Equation (47) is shown together with the commutation error in Figure 4b using $C = 1$. It becomes immediately clear that the scale similarity assumption works less satisfactory for the second derivative compared to the first derivative. Selected results for the second derivatives are summarised in Table 2. The modelling and dynamic procedure are in analogy to the case of the first derivative.

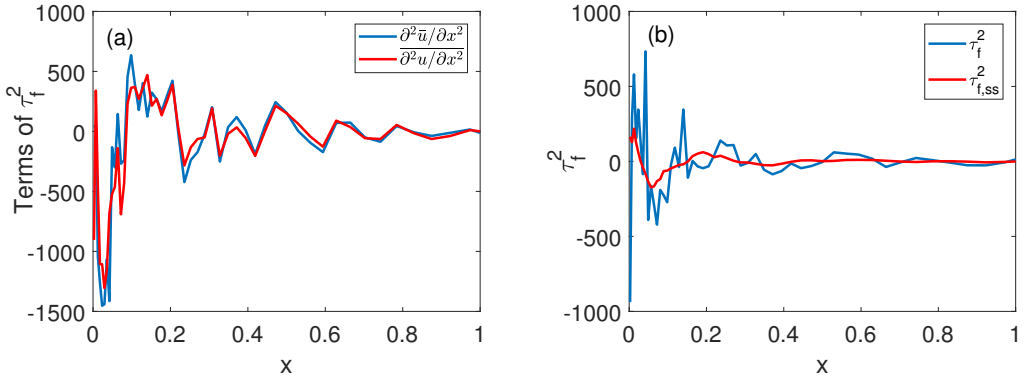

Figure 4. (**a**) (Filtered) second derivatives of the data (filtered data) shown in Figure 2. (**b**) Commutation error given by $\overline{\partial^2 u/\partial x^2} - \partial^2\overline{u}/\partial x^2$ together with scale similarity model for the commutation error, given by Equation (47) using $C = 1$.

While the correlation strengths for the second derivatives are lower compared to the first derivative and also the reduction of RMSE happens to a smaller extend, Table 2 still shows that modelling the commutation error results in a smaller error compared to the commutation error itself especially for small filter width pairs (p_f, p_g).

Table 2. Performance of model $\tau_{f,ss}^2$ for different initial data and different filter sizes (note that the correlation coefficient is independent of the secondary filter). Dynamically determined model coefficient C for different initial data and different f, g filter size pairs (p_f, p_g).

Turb. Length Scale L_{11} **Filter Width Pair (p_f, p_g)**	**5Δx** **(1,2)**	**5Δx** **(5,10)**	**10Δx** **(1,2)**	**10Δx** **(5,10)**
Corr. Coeff.	0.59	0.34	0.50	0.35
Opt. C	1.42	1.12	1.40	1.05
C_{ss} dynamic	1.75	1.45	1.81	1.02
RMSE $(\tau_f^2 - 0)$	1.75	33.41	1.47	30.94
RMSE $(\tau_f^2 - \tau_{f,ss}^2, C = 1)$	1.65	31.30	0.99	28.01
RMSE $(\tau_f^2 - \tau_{f,ss}^2, C_{opt})$	1.18	30.82	0.95	28.00

5. Analysis of Turbulent Channel Flow at $Re_\tau = 590$

Next the relations from Section 2 will be applied to DNS data. For this a-priori analysis a turbulent channel flow DNS at $Re_\tau = 590$ is considered. The equations are solved by using a finite volume technique on a cartesian mesh. The variables are located on a staggered grid. For spatial discretization second order central differences are used. Temporal discretization is an explicit third order, Runge–Kutta-method. The Poisson equation is inverted by using a direct fast solver.

For the channel flow DNS the Reynolds number, based on the wall friction velocity, has been set to $Re_\tau = 590$ similar to the DNS data of Moser et al. [36]. The extension of the computational domain in axial L_x spanwise L_y and vertical L_z direction is $6\delta \times 3\delta \times 2\delta$ where δ is the channel half width. The computational domain is resolved with $512 \times 512 \times 512$ grid points. The grid is stretched in wall normal direction with a factor of $s = 1.0125$ such that $\partial\Delta/\partial x = const$ and $\partial^2\Delta/\partial x^2 = 0$. A fixed theoretical pressure gradient is prescribed in the simulations. This results in a mesh of dimensions $\Delta x_+ = 6.91, \Delta y_+ = 3.46, \Delta z_+ = 7.6$ in the channel center and $\Delta z_+^{min} = 0.32$ at the wall. The filter width parameter has been chosen to $p = 1$ for the primary filter and $p = 2$ for the test filter. To avoid ambiguous definitions of the filter when approaching the wall, all filtering operations stay away from the wall such that with every filter operation the signal becomes a little bit shorter. Nevertheless, for the analysis presented here this is entirely irrelevant. Periodic boundary conditions are applied in axial and spanwise direction,

no slip conditions at the wall. It is worth noting that the above mesh can be considered typical for a channel flow DNS. Using the filter parameter $p = 1$, that is, combining three neighbouring cells into a representative filter volume, can be considered typical for a wall resolved LES mesh. The meshes in homogeneous x, y-directions of channel flow LES/DNS are typically uniform and no commutation errors occur in this direction. Therefore only selected z-components of the different terms of the Navier-Stokes equation have been analysed. It is remarked that in contrast to the analysis in Section 4 where mean values of the signal were zero, the mean axial velocity profile for a channel flow is characterised by strong wall normal gradients in particular in the vicinity to the wall. In other words the signal to be analysed contains the mean velocity contribution which makes it more predictable. Furthermore it is remarked that the wall normal filter width for the DNS and the a-priori LES analysis is very small, presumably much smaller than characteristic turbulent length scales.

First attention is focused on the first order derivatives in the Navier-Stokes equation, that is, the convective term and the pressure gradient. Figure 5a compares the commutation error for the wall normal derivative of convective component $\overline{u}\overline{w}$ with the wall normal gradient of the SGS turbulent flux. Consistent with the analysis of Reference [37] it is found that the commutation error for the convective term can have the same order of magnitude than the SGS contribution. It can further be seen from Figure 5b,d that the scale similarity model represents very well the commutation errors for the term $\partial \overline{u}\overline{w}/\partial z$ and the pressure gradient, where the commutation error for the pressure gradient is much smaller in magnitude. Finally, Figure 5c shows that the dynamically determined model parameter C_{ss} is very close to unity which is consistent with subfigure (b). It is argued that this result is due to the small wall normal filter width (typical for wall bounded LES/DNS) and the velocity profile being dominated by the strong mean gradients.

Terms containing second derivatives, that is, for constant viscosity and density flow the diffusion term and the pressure Laplacian appearing in the Poisson equation for the pressure, will be considered next in Figure 6. Subfigure (a) again shows a very good performance of the scale similarity model (here for the second derivative). Similar observations in regards of the performance for the pressure Laplacian can be seen in Figure 6b. In all cases shown in Figures 5 and 6 the optimal model parameter is very close to unity which has been recovered by the dynamic procedure, but is not explicitly shown here for all terms.

Finally Figure 7 illustrates that Equations (35) and (42) represent reasonable approximations for the commutation error of the first and second wall normal derivative of axial velocity in channel flows. The differential filter given in Equation (36) has been used for filtering the data.

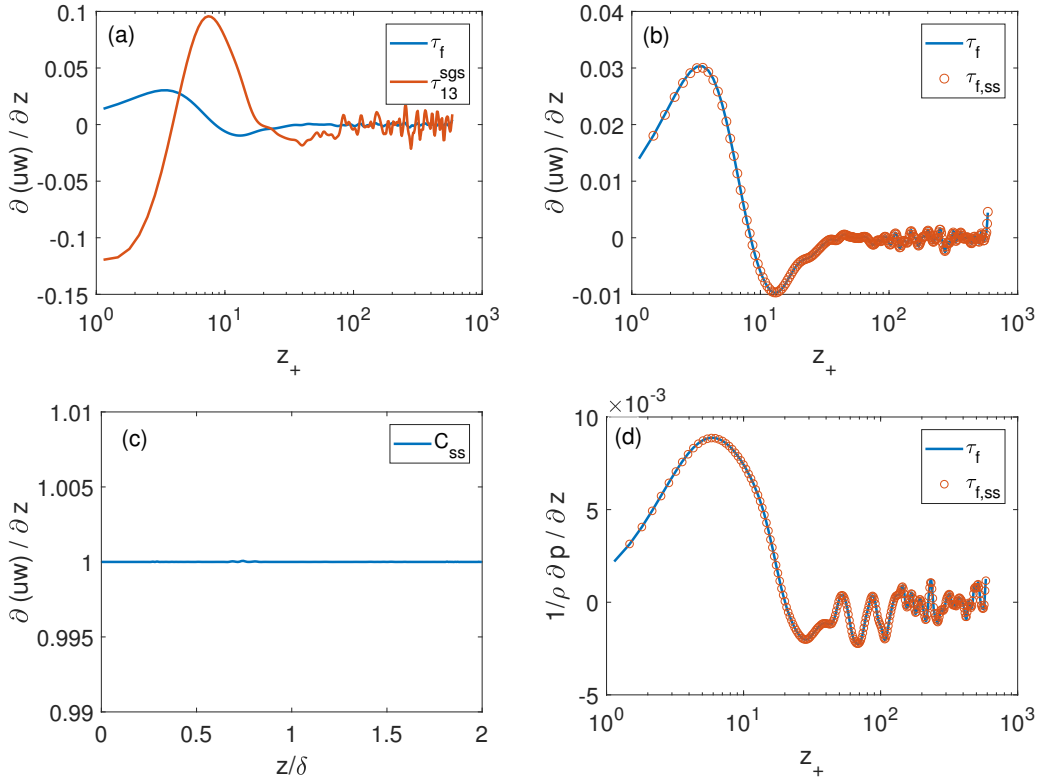

Figure 5. (**a**) Commutation error at primary filter level f for the first derivative $\partial uw/\partial z$ compared to the SGS component $\partial(\overline{uw} - \overline{u}\,\overline{w})/\partial z$ (**b**) Commutation error at primary filter level f for the first derivative $\partial uw/\partial z$ together with the corresponding scale similarity model. (**c**) Dynamic model parameter C_{ss} averaged in both homogeneous directions. (**d**) Commutation error at primary filter level f for the pressure gradient $\partial p/\partial z$ together with the corresponding scale similarity model. Without explicitly mentioning it, all results have been averaged in both homogeneous directions here and in the following figures.

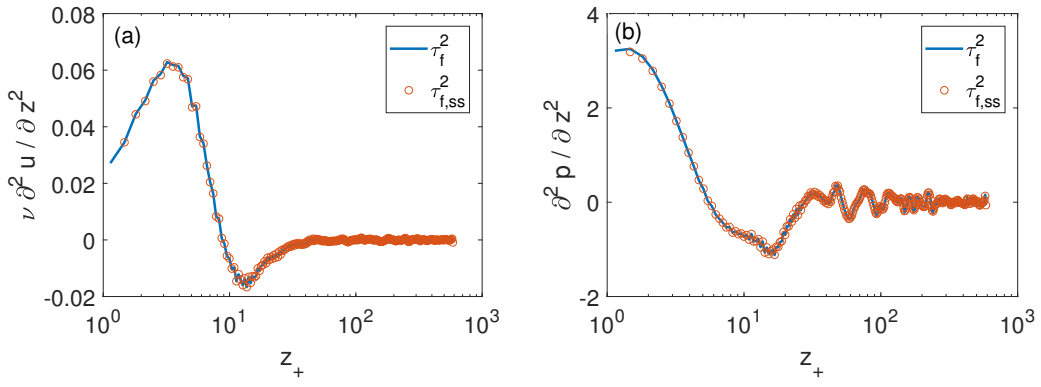

Figure 6. (**a**) Commutation error at primary filter level f for the second derivative (viscous term) $\nu\partial^2 u/\partial z^2$ together with the corresponding scale similarity model. (**b**) Commutation error at primary filter level f for the second derivative $\partial^2 p/\partial z^2$ appearing in the Poisson equation of the projection method together with the corresponding scale similarity model.

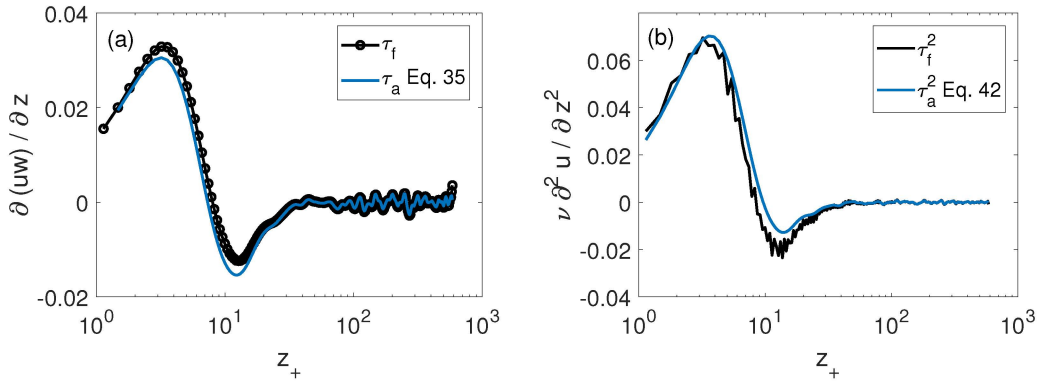

Figure 7. (**a**) Commutation error for $\partial uw/\partial z$ and (**b**) $\nu\partial^2 u/\partial z^2$ with the approximations given by Equations (35) and (42).

6. Conclusions

A large eddy simulation consists of filtering the Navier-Stokes equations in order to compute the large energy carrying motions of the flow while the smaller scales are modelled. The scale separation is formally introduced by a filtering operation. While this approach is very appealing, the filtering operation turns out to be more difficult compared to Reynolds averaging, because of the non-commutativity non only with respect to products but also with respect to derivatives in the case of anisotropic meshes.

A dynamic commutation error model has been produced by generalizing the dynamic modelling procedure. The commutation errors at two different resolution levels are defined and a multiscale identity relating them is derived. All that is in strict analogy with the well known dynamic model. The first results are promising for the future and it is remarked that the same formalism has been extended to second derivatives as well. The framework has been first applied to a synthetic turbulent flow with zero mean values and precisely controllable turbulence characteristics. The results reveal a good correlation strength of the scale similarity model and the dynamic procedure was shown to provide model coefficients close to the optimal model parameter (which cannot be calculated in a real LES in the absence of DNS data).

In a second step an a-priori analysis of a turbulent channel flow has been conducted indicating that the scale similarity models provide a very satisfactory performance with optimal model parameters very close to unity, which again was reproduced by the dynamic procedure. Selected terms of the Navier-Stokes equations have been analysed, showing that the commutation error for the first and second derivative can have a similar order of magnitude than the convective SGS contribution, which is (for the first derivative) consistent with findings from Reference [37] for a different flow configuration and different filtering technique.

In particular the results show, as remarked by Reference [12] that constraints derived from generalizations of the multiscale identities between different resolution levels may provide useful input in the specification of model parameters. Apart future more dedicated applications, the main aim of this short note should be to show the easiness and flexibility of the dynamic approach in very different modelling contexts.

Author Contributions: Conceptualization, M.G. and M.K.; methodology, M.G.; software, M.K.; formal analysis, M.K.; writing—original draft preparation, M.K. and M.G.; writing—review and editing, M.K. and M.G.; visualization, M.K. All authors have read and agreed to the published version of the manuscript.

Funding: This research received no external funding.

Institutional Review Board Statement: Not applicable for studies not involving humans.

Informed Consent Statement: Not applicable for studies not involving humans.

Data Availability Statement: Data available on reasonable request from the authors.

Conflicts of Interest: The authors declare no conflict of interest.

References

1. De Wiart, C.C.; Hillewaert, K.; Bricteux, L.; Winckelmans, G. Implicit LES of free and wall-bounded turbulent flows based on the discontinuous Galerkin/symmetric interior penalty method. *Int. J. Numer. Methods Fluids* **2015**, *78*, 335–354. [CrossRef]
2. Creech, A.; Jackson, A. Hybrid Large Eddy Simulation for low-order Discontinuous Galerkin methods using an explicit filter. *Comput. Phys. Commun.* **2021**, *260*, 107730. [CrossRef]
3. Schoepplein, M.; Weatheritt, J.; Sandberg, R.; Talei, M.; Klein, M. Application of an evolutionary algorithm to LES modelling of turbulent transport in premixed flames. *J. Comput. Phys.* **2018**, *374*, 1166 – 1179. [CrossRef]
4. Reissmann, M.; Hasslberger, J.; Sandberg, R.D.; Klein, M. Application of Gene Expression Programming to a-posteriori LES modeling of a Taylor Green Vortex. *J. Comput. Phys.* **2021**, *424*, 109859. [CrossRef]
5. Janicka, J.; Sadiki, A. Large eddy simulation of turbulent combustion systems. *Proc. Combust. Inst.* **2005**, *30*, 537–547. [CrossRef]
6. Pitsch, H. Large eddy-simulation of turbulent combustion. *Ann. Rev. Fluid Mech.* **2006**, *38*, 453–482. [CrossRef]
7. Ketterl, S.; Klein, M. A-priori assessment of subgrid scale models for large-eddy simulation of multiphase primary breakup. *Comput. Fluids* **2018**, *165*, 64–77. [CrossRef]
8. Klein, M.; Ketterl, S.; Hasslberger, J. Large eddy simulation of multiphase flows using the volume of fluid method: Part 1—Governing equations and a priori analysis. *Exp. Comput. Multiph. Flow* **2019**, *1*, 130–144. [CrossRef]
9. Long, S.; Yang, J.; Huang, X.; Li, G.; Shi, W.; Sommerfeld, M.; Yang, X. Large-eddy simulation of gas–liquid two-phase flow in a bubble column reactor using a modified sub-grid scale model with the consideration of bubble-eddy interaction. *Int. J. Heat Mass Transf.* **2020**, *161*, 120240. [CrossRef]
10. Leonard, A. Energy Cascade in Large-Eddy Simulations of Turbulent Fluid Flows. *Adv. Geophys.* **1974**, *18A*, 237–248.
11. Germano, M.; Piomelli, U.; Moin, P.; Cabot, W. A dynamic subgrid-scale eddy viscosity model. In Proceedings of the 1990 Summer Program, Stanford University, Stanford, CA, USA, December 1990; pp. 5–17. Available online: https://ui.adsabs.harvard.edu/abs/1990stun.proc....5G/abstract (accessed on 30 December 2020).
12. Meneveau, C. Germano identity-based subgrid-scale modeling: A brief survey of variations on a fertile theme. *Phys. Fluids* **2012**, *24*, 121301. [CrossRef]
13. Germano, M. Ten years of the dynamic model. In *Modern Simulation Strategies for Turbulent Flows*; Geurts, B.J., Ed.; Edwards: Philadelphia, PA, USA, 2001; pp. 173–190.
14. Lund, T. On the use of discrete filters for large eddy simulation. In *Annual Research Briefs*; Technical Report; Center for Turbulence Research: Stanford, CA, USA, 1997.
15. Sagaut, P. *Large Eddy Simulation for Incompressible Flows*; Springer: Berlin/Heidelberg, Germany, 1998.
16. Ghosal, S.; Moin, P. The basic equations for the large eddy simulation of turbulent flows in complex geometry. *J. Comput. Phys.* **1995**, *118*, 24–37. [CrossRef]
17. Vasilyev, O.; Lund, T.; Moin, P. A general class of commutative filters for LES in complex geometries. *J. Comput. Phys.* **1998**, *146*, 82–104. [CrossRef]
18. Marsden, A.; Vasilyev, O.; Moin, P. Construction of Commutative Filters for LES on Unstructured MEshes. *J. Comput. Phys.* **2002**, *175*, 584–603. [CrossRef]
19. Ciardi, M.; Sagaut, P.; Klein, M.; Dawes, W. A dynamic finite volume scheme for large-eddy simulation on unstructred grids. *J. Comput. Phys.* **2005**, *210*, 632–655. [CrossRef]
20. John, V. On large eddy simulation and variational multiscale methods in the numerical simulation of turbulent flows. *Appl. Math.* **2016**, *51*, 321–353. [CrossRef]
21. Leonard, S.; Terracol, M.; Sagaut, P. Commutation error in LES with time-dependent filter width. *Comput. Fluids* **2007**, *36*, 513–519. [CrossRef]
22. Franke, J.; Frank, W. Temporal Commutation Errors in Large-Eddy Simulation. *ZAMM J. Appl. Math. Mech.* **2001**, *81*, 467–468. [CrossRef]
23. Geurts, B.; Holm, D. Commutator errors in large-eddy simulation. *J. Phys. A Math. Gen.* **2006**, *39*, 2213–2229. [CrossRef]
24. Lilly, D. A proposed modification of the Germano subgrid-scale closure method. *Phys. Fluids* **1992**, *4*, 633–635. [CrossRef]
25. Bardino, J.; Ferziger, J.H.; Reynolds, W.C. *Improved Turbulence Models Based on Large Eddy Simulation of Homogeneous, Incompressible, Turbulent Flows*; Technical Reports Thermosciences Division; Department Mechanical Engineering, Stanford University: Stanford, CA, USA, 1983.
26. Klein, M.; Kasten, C.; Gao, Y.; Chakraborty, N. A-priori direct numerical simulation assessment of sub-grid scale stress tensor closures for turbulent premixed combustion. *Comput. Fluids* **2015**, *122*, 1–11. [CrossRef]
27. Klein, M.; Chakraborty, N.; Gao, Y. Scale similarity based models and their application to subgrid scale scalar flux modelling in the context of turbulent premixed flames. *Int. J. Heat Fluid Flow* **2016**, *57*, 91–108. [CrossRef]
28. Shamooni, A.; Cuoci, A.; Faravelli, T.; Sadiki, A. New Dynamic Scale Similarity Based Finite-Rate Combustion Models for LES and a priori DNS Assessment in Non-premixed Jet Flames with High Level of Local Extinction. *Flow Turbul. Combust* **2020**, *104*, 233–260. [CrossRef]

29. Klein, M.; Ketterl, S.; Engelmann, L.; Kempf, A.; Kobayashi, H. Regularised, parameter free scale similarity type models for Large Eddy Simulation. *Int. J. Heat Fluid Flow* **2020**, *81*, 108496. [CrossRef]
30. Meneveau, C.; Lund, T.; Cabot, W. A Lagrangian dynamic subgrid-scale model of turbulence. *J. Fluid Mech.* **1996**, *319*, 353–385. [CrossRef]
31. Iovieno, M.; Tordella, D. Variable scale filtered Navier–Stokes equations: A new procedure to deal with the associated commutation error. *Phys. Fluids* **2003**, *15*, 1926–1936. [CrossRef]
32. Chaouat, B. Commutation errors in PITM simulation. *Int. J. Heat Fluid Flow* **2017**, *67*, 138–154. [CrossRef]
33. Germano, M. On the Physical Effects of Variable Filtering lengths and times in LES. In *Advances in LES of Complex Flows*; Springer: Dordrecht, The Netherlands, 2002; pp. 3–11.
34. Germano, M. Differential filters of elliptic type. *Phys. Fluids* **1986**, *29*, 1757–1758. [CrossRef]
35. Klein, M.; Sadiki, A.; Janicka, J. A Digital Filter Based Generation of Inflow Data for Spatially Developing Direct Numerical or Large Eddy Simulations. *J. Comput. Phys.* **2003**, *186*, 652–665. [CrossRef]
36. Moser, R.D.; Kim, J.; Mansour, N.N. Direct numerical simulation of turbulent channel flow up to $Re_\tau = 590$. *Phys. Fluids* **1999**, *11*, 943–945. [CrossRef]
37. van der Bos, F.; Geurts, B.J. Commutator errors in the filtering approach to large-eddy simulation. *Phys. Fluids* **2005**, *17*, 035108. [CrossRef]